J. Fluid Mech. (1978), *vol.* 84, *part* 3, *pp.* 433–453
Printed in Great Britain

Numerical studies of some nonlinear hydrodynamic problems by discrete vortex element methods

By J. C. S. MENG† AND J. A. L. THOMSON
Physical Dynamics, Inc., P.O. Box 1069, Berkeley, California 94701

(Received 11 March 1977)

A class of nonlinear hydrodynamic problems is studied. Physical problems such as shear flow, flow with a sharp interface separating two fluids of different density and flow in a porous medium all belong to this class. Owing to the density difference across the interface, vorticity is generated along it by the interaction between the gravitational pressure gradient and the density gradient, and the motion consists of essentially two processes: the creation of a vortex sheet and the subsequent mutual induction of different portions of this sheet.

Two numerical methods are investigated. One is based upon the well-known Green's function method, which is a Lagrangian method using the Biot–Savart law, while the other is the vortex-in-cell (VIC) method, which is a Lagrangian–Eulerian method. Both methods treat the interface as sharp and represent it by a distribution of point vortices. The VIC method applies the FFT (fast Fourier transform) to solve the stream-function/vorticity equation on an Eulerian grid, and computational efficiency is further improved by using the reality properties of the physical variables.

Four specific problems are investigated numerically in this paper. They are: the Rayleigh–Taylor instability, the Saffman–Taylor instability, transport of aircraft trailing vortices in a wind shear, and the gravity current. All four problems are solved using the VIC method and the results agree well with results obtained by previous investigators. The first two problems, the Rayleigh–Taylor instability and the Saffman–Taylor instability, are also solved by the Green's function method. Comparisons of results obtained by the two methods show good agreement, but, owing to its computational economy, the VIC method is concluded to be the better method for treating the class of hydrodynamic problems considered here.

1. Introduction

The formation of ring or line-pair vortices following injection of a blob of fluid into a medium at rest is a very common phenomenon. Some well-known examples include the classic 'smoke ring' and its two-dimensional analogue in aircraft wakes. When a spherical volume of air is heated at constant pressure as a result of a point release of energy, the hot bubble of gas rises and is typically observed to develop into a toroidal ring-vortex configuration by the time it has risen a distance of the order of its initial diameter. The two-dimensional analogue of this axisymmetric motion can occasionally be observed in bent-over chimney plumes, where the hot gas emanating from the chimney is stretched horizontally into a long cylinder by an ambient wind. When the air

† Present address: Science Applications, Inc., P.O. Box 2351, La Jolla, California 92037.

is calm, this long cylinder of hot gas can be observed to develop into two parallel line vortices as it floats upwards.

In the case of smoke-ring ejection and the aircraft wake the initial motion consists of a distributed sheet of vorticity embedded in a hydrodynamically irrotational flow. The subsequent development of the motion in an incompressible fluid can be thought of as a mutual induction or interaction between the various sections of the vortex sheet. In the two-dimensional case in the absence of viscosity, vorticity is a transferable quantity and no new vorticity is created during the ensuing motion. In the case of buoyant motions (rising bubble, bent-over chimney plume), the initial state may be approximated as an irrotational one, with zero vorticity. The interaction between the gravitational pressure gradient and the density gradients provides a source of vorticity and the motion consists essentially of two processes: the creation of a vortex sheet or a vortex layer as a result of buoyancy and the subsequent mutual induction of different portions of this sheet. The induction phenomenon closely parallels the development in non-buoyant injection flows. In the buoyant phenomena, the mechanics of the vorticity generation are essentially those that give rise to the well-known Rayleigh–Taylor instability.

The motion of the vortex sheet in the ejection class of flows is closely related to the Kelvin–Helmholtz instability which occurs at the interface between two fluids in relative motion. In this case the interface (vortex sheet) is unstable to the development of line vortices whose axes are perpendicular to the velocity-difference vector. In the case of a wakelike flow, which can be approximated by two parallel vortex sheets of opposite sign, this instability results in the development of the well-known Kármán vortex street.

There is another class of flows which, though not always resulting in vortex formation, is quite similar in its hydrodynamics to the flows discussed above. These flows occur in porous media where the inertia forces are negligible compared with the viscous forces. Here the mechanisms driving the motion are again either the initial vorticity or the vorticity induced as a result of buoyant or pressure-gradient forces. Examples of this class of flows include the motion of a variable-density incompressible fluid through a porous medium under the influence of gravity or a pressure gradient. In the case of a heavy liquid overlying a light liquid, the Rayleigh–Taylor mechanism is operative and the fluid will develop a motion commonly known as the Saffman–Taylor instability in a porous medium.

In this paper we consider a class of two-dimensional flows in the special case where the flow consists of two incompressible liquids of different density separated by a sharp interface with or without shear across it. The objective of this paper is to develop simple numerical treatments of this restrictive class in a fashion that makes clear the similarities and differences between the various phenomena.

Major characteristics of this class of flows are that the flow equations are elliptic in nature and that there is a sharp interface. The former requires the entire flow field to be calculated at once; the latter necessitates proper removal of the mathematical singularity. These problems and the apparent nonlinearity have hindered effective numerical studies in the past.

The crux of this paper is to demonstrate how those difficulties can be removed. One aspect of the success is realized by recognizing that, even though the flow equation is elliptic mathematically, physically the flow is dominated by the distributed vorticity

on the sharp interface. Therefore it is wasteful to compute the passive portion of the flow (away from the interface) which stays passive and irrotational. In fact, it is advantageous to treat the problem from the point of view of the sharp interface since this reduces a two-dimensional plus time problem into a one-dimensional plus time problem, where the single dimension is along the interface. Another aspect of the success lies in removing the mathematical singularity. This is accomplished by either specifying a core radius for all the discrete vortex elements (Green's function method) or computing the velocity on an Eulerian grid (the vortex-in-cell method).

In the Green's function method, one discretizes the interface and calculates the interactions among the discrete vortices. It is a precise simulation of a real problem and it is a limiting model for the sharp interface; however, the total number of operations is proportional to N^2, where N is the number of discrete vortices on the interface, which becomes costly as N increases.

The alternative is to construct a numerical method capable of subgrid spatial resolution (sharp interface) which generates a solution independent of the core radius of the discrete vortex elements. Neither a pure Eulerian nor a pure Lagrangian method can be satisfactory, since the former cannot resolve the sharp interface and the latter generates meaningful solutions only when a non-zero vortex core radius is applied. A Lagrangian–Eulerian method is the only alternative. A vortex-in-cell (VIC) method is therefore developed here in which one discretizes the interface into discrete vortex elements with zero core radius, but calculates the velocity field from the vorticity stream function on an Eulerian grid. Since the stream function is independent of the vortex core radius, the mathematical singularity inherent in the Green's function method is avoided. On the other hand, the density or the vorticity field is calculated in a Lagrangian fashion from the discrete vortex elements so that the sharp interface is preserved. The vorticity stream function is found by the fast Fourier transform (FFT) method, which also uses the reality of the physical variables. Computational economy is achieved both because of this and because the number of operations in the FFT is proportional to $M_x M_y \ln (M_x M_y)$, where M_x and M_y are the numbers of mesh points in the x and y directions, which are independent of the total number of discrete vortices N. Therefore the VIC method can treat a problem with a sharp interface using a very large number of vortices without increasing the computational effort, which is not possible by the Green's function method.

In § 2, the rate of change of the circulation carried by each discrete vortex element will be derived for both inviscid fluid and viscous fluid in a porous medium. Section 3 describes the numerical aspects of both Green's function and VIC methods. Section 4 discusses the numerical results obtained for various physical problems.

2. Formulation of the problem

In the present analysis we shall be concerned with fluids where the fractional variations of the density and viscosity are small ($\Delta\rho/\rho, \Delta\nu/\nu \ll 1$). Some aspects of the large density difference across the interface with the consideration of surface-tension effects will be discussed in the future.

2.1. *Inviscid fluids*

For inviscid fluids the vorticity equation takes the form

$$d\boldsymbol{\Omega}/dt = -\nabla\rho^{-1} \times \nabla p \tag{1}$$

and to first order in the density difference (since $\nabla p = \rho_0 \mathbf{g} + O(\Delta\rho/\rho_0)$ and if $\mathbf{g}$ is in the $-y$ direction

$$\frac{d\boldsymbol{\Omega}}{dt} = \frac{\nabla\rho}{\rho_0} \times \mathbf{g} = -\frac{g}{\rho_0}\frac{\partial\rho}{\partial x}\mathbf{n}_z. \tag{2}$$

For two-dimensional motion in the x, y plane, the vorticity is effectively a scalar (i.e. has only a z component along $\mathbf{n}_z$). Of particular interest is the case of two uniform immiscible fluids of slightly differing density. In this case, vorticity is generated only at the interface between the two fluids; the remainder of the flow remains irrotational.

The total circulation

$$\boldsymbol{\Gamma}_i = \int \boldsymbol{\Omega}_i \, dx' \, dy'$$

of a given (ith) fluid element is determined by

$$d\boldsymbol{\Gamma}_i/dt = g\rho_0^{-1}(\rho_- - \rho_+)\,\Delta y_i \mathbf{n}_z, \quad \rho_0 = \tfrac{1}{2}(\rho_+ + \rho_-), \tag{3}$$

where ρ_+ and ρ_- are the densities to the right and left of the interface, Δy_i is the vertical dimension of the fluid element and $\mathbf{n}_z$ is a unit vector perpendicular to the plane of motion.

A convenient numerical analysis of the evolution of the fluid motion can be obtained by dividing up the interface into a number of discrete vortex elements and approximating the circulation of each element as being concentrated into a line vortex having circulation Γ_i. The quantity Δy_i is then to be interpreted as the vertical separation between adjacent vortices. The evaluation of the fluid motion then reduces to the problem of following the motion of the individual discrete vortices. The velocity of the ith vortex is a sum over contributions from all other vortices:

$$\frac{d\mathbf{r}_i}{dt} = \mathbf{u}_i = \sum_{j \neq i}^{N} \frac{\boldsymbol{\Gamma}_j}{2\pi} \times \frac{(\mathbf{r}_i - \mathbf{r}_j)}{|\mathbf{r}_i - \mathbf{r}_j|^2}. \tag{4}$$

This equation of motion, plus the relation determining the circulation growth rate [equation (3)], in which Δy_i is replaced by $\frac{1}{2}(y_{i+1} - y_{i-1})$, yields a direct deterministic procedure for following the motion; this is termed the Green's function method.

Instead of the Green's function form for the velocity field, the velocity may be expressed in terms of a stream function $\boldsymbol{\Psi}$ defined on an Eulerian grid,

$$\mathbf{u} = \nabla \times \boldsymbol{\Psi}, \tag{5}$$

with $\boldsymbol{\Psi}$ defined such that $\nabla . \boldsymbol{\Psi} = 0$ (the vanishing of $\nabla . \boldsymbol{\Psi}$ is automatic in two-dimensional motion). The stream function satisfies a Poisson equation with the vorticity as the source function:

$$\nabla^2 \boldsymbol{\Psi} = -\boldsymbol{\Omega}. \tag{6}$$

Equations (3), (5) and (6) form another deterministic procedure for following the motions; this is called the vortex-in-cell (VIC) method.

2.2. *Viscous flows in a porous medium*

When the viscous forces dominate the inertial forces, and for the flow of a fluid between two parallel plates, the flow is locally Poiseuille-like and the viscous term is dominated by the curvature of the velocity profile in the direction normal to the plates, so that

$\nabla^2\mathbf{u} \simeq -8\mathbf{u}/d^2$, where d is the plate separation and $\mathbf{u}$ is the centre-line velocity. We then have the following momentum equation:

$$\mathbf{u} = -\frac{d^2}{8\rho\nu}\nabla p + \frac{d^2}{8\nu}\mathbf{g}. \tag{7}$$

Taking the curl of (7), we obtain for the vorticity

$$\zeta = \frac{d^2}{8}\left[-\nabla\left(\frac{1}{\rho\nu}\right)\times\nabla p + \nabla\left(\frac{1}{\nu}\right)\times\mathbf{g}\right]. \tag{8}$$

To first order in the density and viscosity variations, ∇p may be replaced by ∇p_0, where $\nabla p_0 = -8\rho_0\nu_0/d^2\mathbf{U}_0 + \rho_0\mathbf{g}$, and

$$\zeta = -\frac{\nabla(\rho\nu)}{\rho_0\nu_0}\times\mathbf{U}_0 + \frac{\nabla\rho}{\rho_0\nu_0}\times\left(\frac{d^2\mathbf{g}}{8}\right). \tag{9}$$

For two uniform fluids separated by a sharp interface, and if the vectors $\mathbf{U}_0$ and $\mathbf{g}$ are in the same direction, the total circulation Γ_i of a given (ith) fluid element can be determined from

$$\Gamma_i = \left[\left(\frac{\mu_+ - \mu_-}{\mu_0}\right)U_0 - \left(\frac{\rho_+ - \rho_-}{\rho_0}\right)\right]\frac{d^2g}{8\nu_0}\Delta y_i, \tag{10}$$

where $\mu_\pm = (\rho\nu)_\pm$ are the viscosities of the fluids to the right and left of the interface respectively.

Equations (10) and (4) form a deterministic procedure for following the motion; this is the Green's function method for the porous medium. Equations (10), (5) and (6) form the other procedure, namely the VIC method for a porous medium.

2.3. *Non-dimensionalization of the equations*

Equations of motion for both inviscid and viscous fluids in a porous medium will be made dimensionless in this section.

When there is no stratification, (4) is reduced to dimensionless form by introducing the following characteristic dimensions.

Length: R = a representative length, initial cylinder radius or wavelength.

Time: $T = 2\pi R^2/\Gamma_0$.

Circulation: Γ_0 = total circulation assumed to be distributed on the interface or the vortex sheet.

When there is density variation, (3) and (4) are reduced to dimensionless form by introducing the following characteristic dimensions.

Length: R = the initial cylinder radius or wavelength.

Time: $T = [g(\Delta\rho/\rho_0)/2\pi R]^{-\frac{1}{2}}$.

Circulation: $\Gamma_0 = [2\pi g(\Delta\rho/\rho_0)\,R^3]^{\frac{1}{2}}$.

In terms of the dimensionless distances $\xi = x/R$ and $\eta = y/R$, the dimensionless time $\tau = t/T$ and the dimensionless circulation $\gamma = \Gamma/\Gamma_0$, the equations of motion become

$$d\gamma_i/d\tau = \Delta\eta_i, \tag{11}$$

$$\frac{d\xi_i}{d\tau} = -\sum_{j\neq i}^{N} \gamma_j(\eta_j-\eta_i)/[(\xi_j-\xi_i)^2+(\eta_j-\eta_i)^2], \tag{12}$$

$$d\eta_i/d\tau = \sum_{j\neq i}^{N} \gamma_j(\xi_j-\xi_i)/[(\xi_j-\xi_i)^2+(\eta_j-\eta_i)^2], \tag{13}$$

where

$$\Delta\eta_i = \tfrac{1}{2}(\eta_{i+1}-\eta_{i-1}).$$

For viscous fluids in a porous medium (11) is replaced by the non-dimensional version of (10). In this case, the following characteristic dimensions are defined.

Length: R = the initial cylinder radius or wavelength.

Time: $T = 2\pi R^2/\Gamma_0$.

Circulation: $\Gamma_0 = \left(\frac{\Delta\mu}{\mu_0}U_0 - \frac{\Delta\rho}{\rho_0}\frac{d^2g}{8\nu_0}\right)R.$

In terms of the dimensionless distances $\xi = x/R$ and $\eta = y/R$, the dimensionless time $\tau = t/T$ and the dimensionless circulation $\gamma = \Gamma/\Gamma_0$, the equations of motion (4) and (10) for the viscous flow in a porous medium become

$$\gamma_i = \Delta\eta_i, \tag{14}$$

$$\frac{d\xi_i}{d\tau} = -\sum_{j\neq i}^{N} \gamma_j(\eta_j-\eta_i)/[(\xi_j-\xi_i)^2+(\eta_j-\eta_i)^2] \quad \text{[equation (12)]},$$

$$\frac{d\eta_i}{d\tau} = \sum_{j\neq i}^{N} \gamma_j(\xi_j-\xi_i)/[(\xi_j-\xi_i)^2+(\eta_j-\eta_i)^2] \quad \text{[equation (13)]},$$

where

$$\Delta\eta_i = \tfrac{1}{2}(\eta_{i+1}-\eta_{i-1}).$$

Equations (12) and (13) are repeated here for clarity.

Equations (11), (12) and (13) form the deterministic set for the inviscid case, while (14), (12) and (13) form the equivalent set for the viscous flow in a porous medium. This completes the formulation of both cases in terms of the Green's function method.

Similar non-dimensionalizations can be carried out for the stream function $\psi = \Psi/\Gamma_0$ for the VIC method and will not be described in detail here.

3. Some aspects of the numerical methods

3.1. *Description of the Green's function method*

Formulation of the finite core radius. It was pointed out by Chorin & Bernard (1973) that, unless a finite core radius is used, the accuracy of the discrete vortex element method does not improve with an increment of the total number of vortex elements. The finite core radius is employed here by using an algebraic relation which not only satisfies the physical smoothing requirement, but also eliminates the test procedure to find out whether the point of concern falls within the core radius or not.

The denominator in the velocity relation (4) is modified by replacing $|\mathbf{r}_i-\mathbf{r}_j|^2$ by $|\mathbf{r}_i-\mathbf{r}_j|^2+r_c^2$, where r_c is the core radius. For $|\mathbf{r}_i-\mathbf{r}_j| \ll r_c$, therefore, in the core, the

velocity grows linearly with respect to the distance $|\mathbf{r}_i - \mathbf{r}_j|$, and falls off as $1/|\mathbf{r}_i - \mathbf{r}_j|$ if $|\mathbf{r}_i - \mathbf{r}_j| \gg r_c$. In an accurate simulation of a physical phenomenon, the value of r_c should be matched to experimental data, however the solution should not depend critically upon the arbitrary choice of a non-zero r_c value (Chorin & Bernard 1973). For all the calculations reported here, we set $r_c = R/N$, where N is the total number of discrete vortex elements on the interface.

Repacking the vortices. One problem which is commonly associated with a Lagrangian calculation is the continual addition or removal of particles from the calculation. Depending upon the physical nature of the problem, particles may become crowded and yield unrealistically high gradients of flow variables or the number of particles in a region of interest may be so low that no realistic representation of flow is possible. From the point of view of maintaining a uniform accuracy, a procedure which can rearrange, add or delete particles as necessary must be applied. It is also desirable from an economic point of view since a number larger than a limiting number of vortices will not improve accuracy, but a number smaller than a limiting number of vortices will reduce accuracy. Without being committed to using a large number of vortices throughout the computation, there is no alternative but to adopt a repacking procedure. Since the vortices do carry physical variables (vorticity) the repacking procedure must be based upon the laws of conservation. For the present calculation, these are the vorticity and the centroid of the vorticity.

The method adopted here is to add or delete a vortex element when the separation distance between neighbouring vortices exceeds or falls below a preset limit, then redistribute the vorticity among the added and the original vortices to satisfy the conservation laws. To be specific, assume that between the ith and $(i+1)$th vortices one vortex is added. The circulation of the new vortex will be $\frac{1}{3}(\Gamma_i + \Gamma_{i+1})$ and the circulation of the original particles is reduced to $\frac{2}{3}\Gamma_i$ and $\frac{2}{3}\Gamma_{i+1}$, accordingly. The new vortex position is determined by a linear relation which keeps the centroid of the vorticity unchanged.

Another method, although it has not been applied in the present calculations, is to impose an equal separation distance between the vortices at all times. This separation distance can either be constant or vary as a function of time. Then the vortices are rearranged accordingly, and the physical variables, circulation and spatial positions are interpolated using a cubic spline interpolation polynomial over all the vortices. Through numerical experiments which were discussed in Meng (1977), it is evident that this repacking procedure is more effective in removing 'spurious' numerical errors. The reason for the success with an equal separation distance between the discrete vortex elements is explained in Fink (1973).

3.2. *Description of the VIC method*

Several numerical procedures required in the application of the VIC method will be described below. Owing to the possible broad numerical aspect of each procedure, we shall concentrate on description of the actual procedures applied.

Bilinear interpolation. As is true for all Lagrangian–Eulerian methods, an interpolation method must be applied back and forth between the Lagrangian particles and the fixed Eulerian grids. In the VIC method, we have applied the bilinear interpolation method.

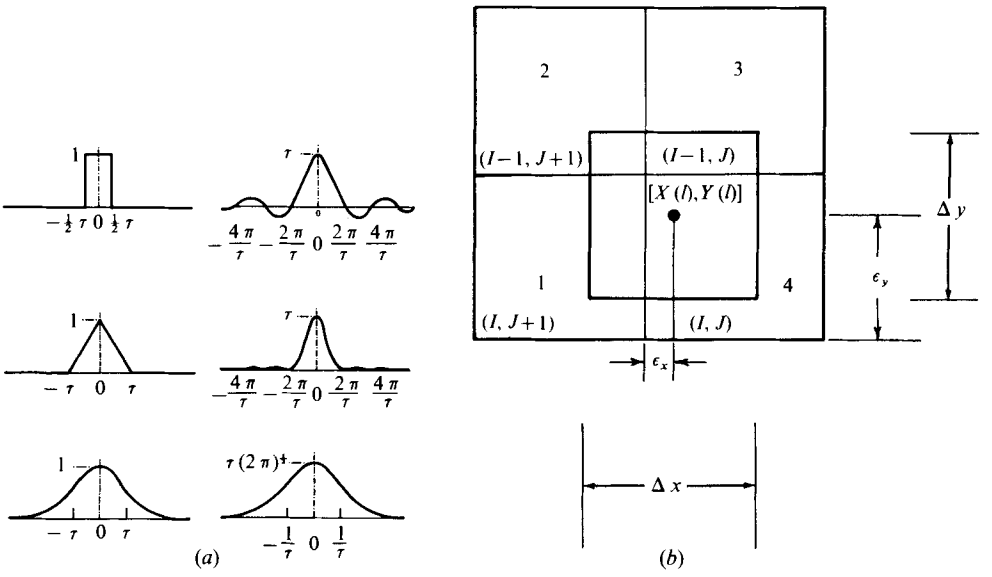

FIGURE 1

Spreading. One characteristic length in the VIC method is the cell size for the FFT method. When the circulation carried by the vortices is spread over a rectangle instead of the infinitesimal area covered by a point, additional dimensions are introduced. This will alleviate the singularity associated with the particle representation. Consider the three distributions shown (with their Fourier transforms) in figure 1 (*a*): the top one is a step function with narrow width and its Fourier transform will produce noise of very high frequency; for the second distribution, less noise is produced at high frequency as a result of spreading the quantity linearly; in the last case, which is the best representation, no noise is generated at high frequency. We have adopted here a distribution similar to the last case; figure 1 (*b*) illustrates the relationship between the mesh, identified by indices I and J, and the lth particle, located at $[X(l), Y(l)]$. We spread the vorticity over a rectangle with the dimensions Δx and Δy of one cell, and make sure that there is approximately one particle per cell throughout the computation, and assume a vorticity distribution according to

$$1/\{1+[(x-X(l))/\Delta_x]^2\}\{1+[(y-Y(l))/\Delta_y]^2\},$$

where $\Delta_x = \frac{1}{3}\Delta x$ and $\Delta_y = \frac{1}{3}\Delta y$ are the half-widths characterizing the spreading. Then the weighting factors are obtained by integrating the above relation over the overlapping area in each cell. The spreading of the physical quantities according to the above relation was found to be effective in removing irregular motion of the vortices. The effect is similar to that of the finite core radius used in the Green's function method, since it introduces a mesh-independent length scale over which one can distribute the vorticity arbitrarily. This greatly enhances the capability of the VIC method to deal with flows with high gradients.

Use of the reality of the physical variables. Since all physical variables in the problem are real, their Fourier components should satisfy the relation

$$\Psi^*(\mathbf{k}) = \Psi(-\mathbf{k}),$$

where the asterisk represents complex conjugation. This property has been fully used in the VIC method by calculating the first half of the Fourier components, i.e. $\Psi(k_x, k_y)$ for $k_x \geqslant 0$, only. The second half of the Fourier components, i.e. that for $k_x < 0$, is obtained by complex conjugation. That is, letting $k_x > 0$, we have

$$\Psi(-k_x, k_y) = \Psi^*(k_x, -k_y), \quad \Psi(-k_x, -k_y) = \Psi^*(k_x, k_y).$$

The Fourier components of $\mathbf{u} = \nabla \times \boldsymbol{\Psi}$, or $\mathbf{u}(\mathbf{k}) = -i\mathbf{k} \times \boldsymbol{\Psi}(\mathbf{k})$, where $\boldsymbol{\Psi} = (0, 0, \Psi)$, are obtained similarly. For example, the Fourier components of the horizontal velocity are

$$u(k_x, k_y) = -ik_y \Psi(k_x, k_y), \quad u(-k_x, k_y) = -ik_y \Psi^*(k_x, -k_y).$$

Imposition of periodic boundary conditions. The efficiency of the FFT is achieved with a periodic boundary condition. The domain dimensions are taken to be periodic lengths so that images exist one periodic length apart even though they are not visible in the computational domain. This also implies that, when a vortex is swept out of the flow domain at one side, another vortex must be introduced into the flow domain a distance of one periodic length away from the original position. To make certain that the image exerts no significant influence upon the flow, this in general requires the region of interest to be centred in the computational domain.

Damping. All physical problems treated by the VIC method are basically unstable, i.e. amplification of small perturbations (or numerical errors) always occurs. It is necessary to eliminate errors generated by the numerical procedure in order to obtain a smooth solution. One of the error sources is the finite mode Fourier transform; this error is known as aliasing error and was discussed in detail by Cooley & Tukey (1965). Since the mesh size $(\Delta x, \Delta y)$ set the highest wavenumber representable by the Fourier series, all high wavenumber components must stay small throughout the calculation. This is achieved conveniently through a damping procedure in the Fourier space. We have applied the damping function

$$\exp\left\{-\beta\left[\left(\frac{k_x \Delta x}{2\pi}\right)^4 + \left(\frac{k_y \Delta_y}{2\pi}\right)^4\right]\right\}$$

and found $\beta = 2$ sufficient in very unstable flows. However, its effect on the conservation of circulation or momentum has not been investigated.

4. Numerical computations by the discrete vortex methods

Vortex consideration furnishes a powerful ally in attacking many nonlinear rotational hydrodynamic flows. In this context, we shall establish the accuracy and efficiency of such a numerical approach by emphasizing the manner in which motion is generated by the vorticity and how the subsequent evolution develops.

4.1. *Rise of a buoyant cylinder (Rayleigh–Taylor instability)*

Scorer (1958, p. 194) suggested that the behaviour of plumes of smoke which have been bent over by a crosswind and become nearly horizontal can conveniently be discussed in terms of a line source of buoyancy. Turner (1959) studied this in a water channel and observed that plumes bent over in this way tend to split sideways into two concentrated regions with a clear space between them. He found that the flow

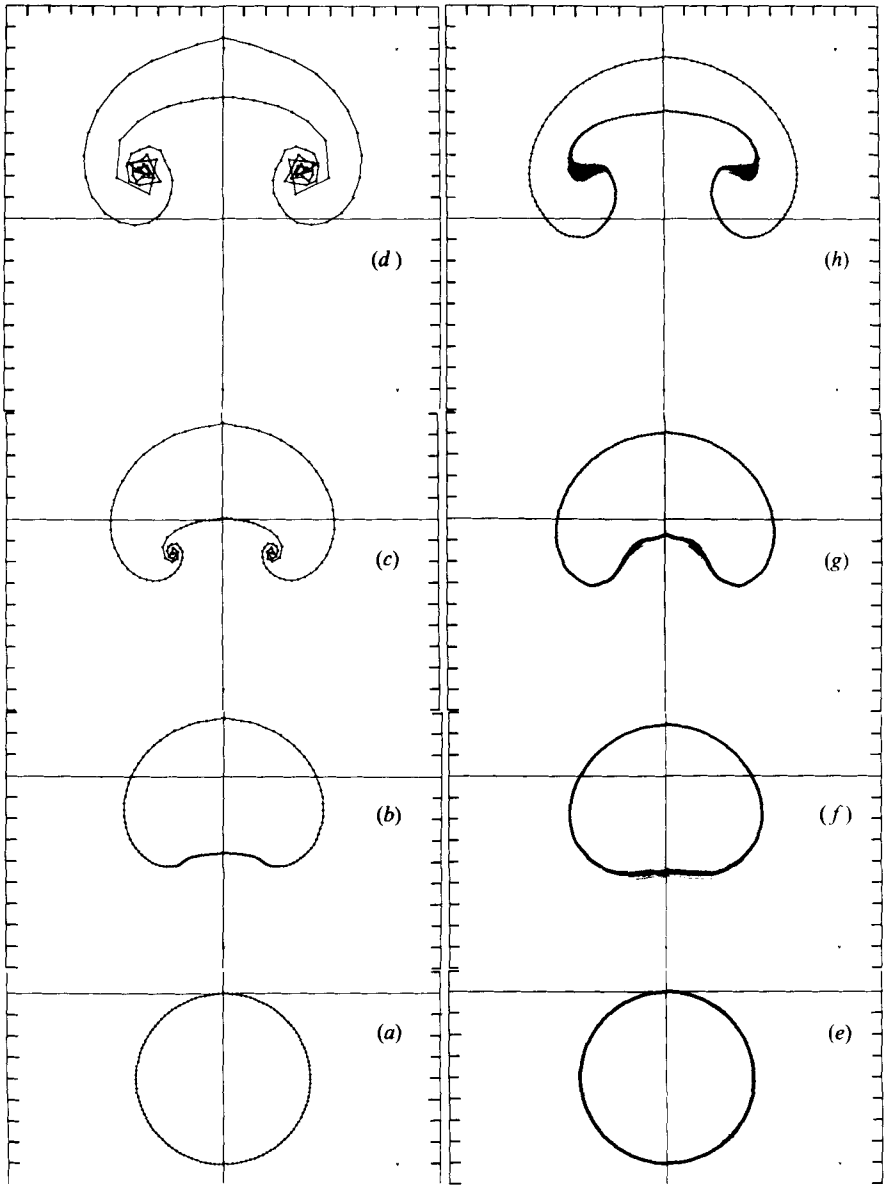

FIGURE 2. Rise of a buoyant cylinder. (*a*)–(*d*) Results of the Green's function method with 61 vortices on the right-hand semicircle. (*e*)–(*h*) Results of the VIC method with 200 vortices on the right-hand semicircle. Non-dimensionalized time (defined in §2.3): (*a*), (*e*) 0; (*b*), (*f*) 0·72; (*c*), (*g*) 1·00; (*e*), (*h*) 1·56.

in planes perpendicular to the axis of the plume is very like that in a vortex pair, with a region of fast rise in the centre and slower regions on each side.

Equations (11)–(13) have been used to calculate the time-dependent motion in two dimensions following the release of an initially uniform circular cylinder of light fluid in a homogeneous heavier fluid. Since the density gradients in this example are confined to the (deforming) surface of the cylinder, the motion may be traced by following

the history of the vortex sheet which comprises the cylinder boundary initially (see figure 2*a*). The results of the calculation are shown in figures 2(*a*)–(*d*). The cylinder boundary at time zero was divided uniformly into N discrete vortices (61 on the semicircle). The velocity of each point was calculated at successive time increments according to (12) and (13). The circulation of each point was calculated from (11) as a function of time, the initial values being taken equal to zero.

The initial motion of the cylinder is simply an upward displacement without sensible distortion. By the time the net displacement is of the order of one half of the initial cylinder radius, the beginning of vortex development is evident (figure 2*b*). The vortex appears to be well developed by the time the buoyant region has risen about one diameter (figure 2*c*). By this time, most of the vorticity is concentrated in the vortex region. The rate of change of the total circulation of this region is obtained by summing (11) over the entire vortex sheet:

$$\frac{d}{d\tau}\left(\sum_i \gamma_i\right) = \delta\eta,$$

where $\delta\eta$ is the thickness of the cap on the axis of symmetry. Thus the value of the vortex circulation grows during the vortex development but saturates when the vortex has developed fully. The subsequent motion (after vortex formation) of the buoyant and entrained material has been discussed by others (particularly by Turner 1959; also by Fohl 1967). It is important to point out here that the vortex interaction process is responsible for the flow entrainment, not turbulence; the basic motion is an inviscid rotational flow, not necessarily a turbulent motion. Although the present calculation was carried out for a cylindrical configuration, essentially similar results can be anticipated for a spherical configuration.

When the cylinder (see figure 2*d*) has risen more than one diameter, the set of point vortices forms an irregular distribution within a finite cloud. The original vortex sheet is now so convoluted as to be impossible to follow. Although the numerical model cannot be a good model of the small-scale structure at such times, it is important to understand whether the large-scale motion agrees with theoretical analysis.

Turner (1959) has shown that the circulation of each vortex approaches a constant value after vortex formation. This may be seen from Kelvin's theorem, which states that, for any closed circuit display C,

$$d\Gamma/dt = \oint_C (1/\rho)\nabla p.d\mathbf{s}.$$

After vortex formation, the density along a path threading the centre of the vortex is essentially constant and equal to the ambient value, and $d\Gamma/dt \to 0$. When Γ is constant, the rise velocity varies inversely as the separation of the vortex pair: $V \propto 1/R$. The upward momentum increases at a constant rate $d(MV)/dt = F_B$, where F_B is the (constant) buoyant force and M is total mass in the vortex. Since M is proportional to R^2 in two dimensions and RV is constant, the separation R increases linearly with time: $R \sim t$. Since the rise velocity of the vortex pair varies as Γ/R, the net rise distance y increases logarithmically (in two dimensions) with time: $y \sim \ln t$. In figure 3 we show that the time dependence of the width and height of the rising vortex pair agrees well with the expected dependence.

In three dimensions the expansion rate will have a different time dependence. Since here the mass varies as R^3, the momentum equation reduces to $dR^2/dt \sim$ constant

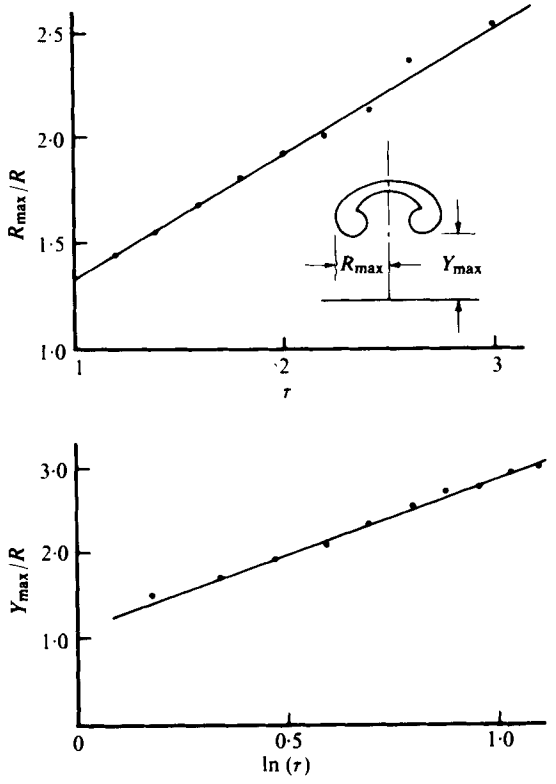

FIGURE 3. Width and height of a buoyant cylinder *vs.* time.

after torus formation (when $RV \sim$ constant). Here $R \sim t^{\frac{1}{2}}$ and $dz/dt \sim t^{-\frac{1}{2}}$. Thus the radius of the torus increases linearly with height ($R \sim z$).

If the vortex-in-cell (VIC) method is applied to solve the problem, a vortex system of much larger numbers of particles can be employed, taking essentially the same amount of computation time. For example, in the Green's function approach, using 61 vortices took 0·246 s per time step. The VIC method took 0·426 s per step, with 591 vortices, while the same approach took 0·31 s per step with only 41 vortices. All calculations were performed on a CDC 7600. Figures 2 (*e*)–(*h*) show the results obtained by the VIC method using 200 vortices over the same period as that in figures 2 (*a*)–(*d*).

Comparing figures 2 (*a*)–(*d*) with figures 2 (*e*)–(*h*) shows that the large-scale motion is reproduced closely by the VIC method. The small-scale motion generated by the Green's function method, however, cannot be reproduced by the VIC method owing to the finite mode Fourier transform. Therefore this indicates that no advantage can be realized by using the VIC method in a numerical calculation where no more than 50–100 discrete vortices are required to resolve the flow motion.

4.2. *Saffman–Taylor instability*

Long narrow convecting cells, i.e. 'salt fingers', are commonly observed when hot salt water is poured over cold fresh water. A very similar phenomenon occurs at the interface of two superposed viscous fluids when they are forced by gravity or an imposed pressure gradient through a porous medium. Practical examples, in addition to those

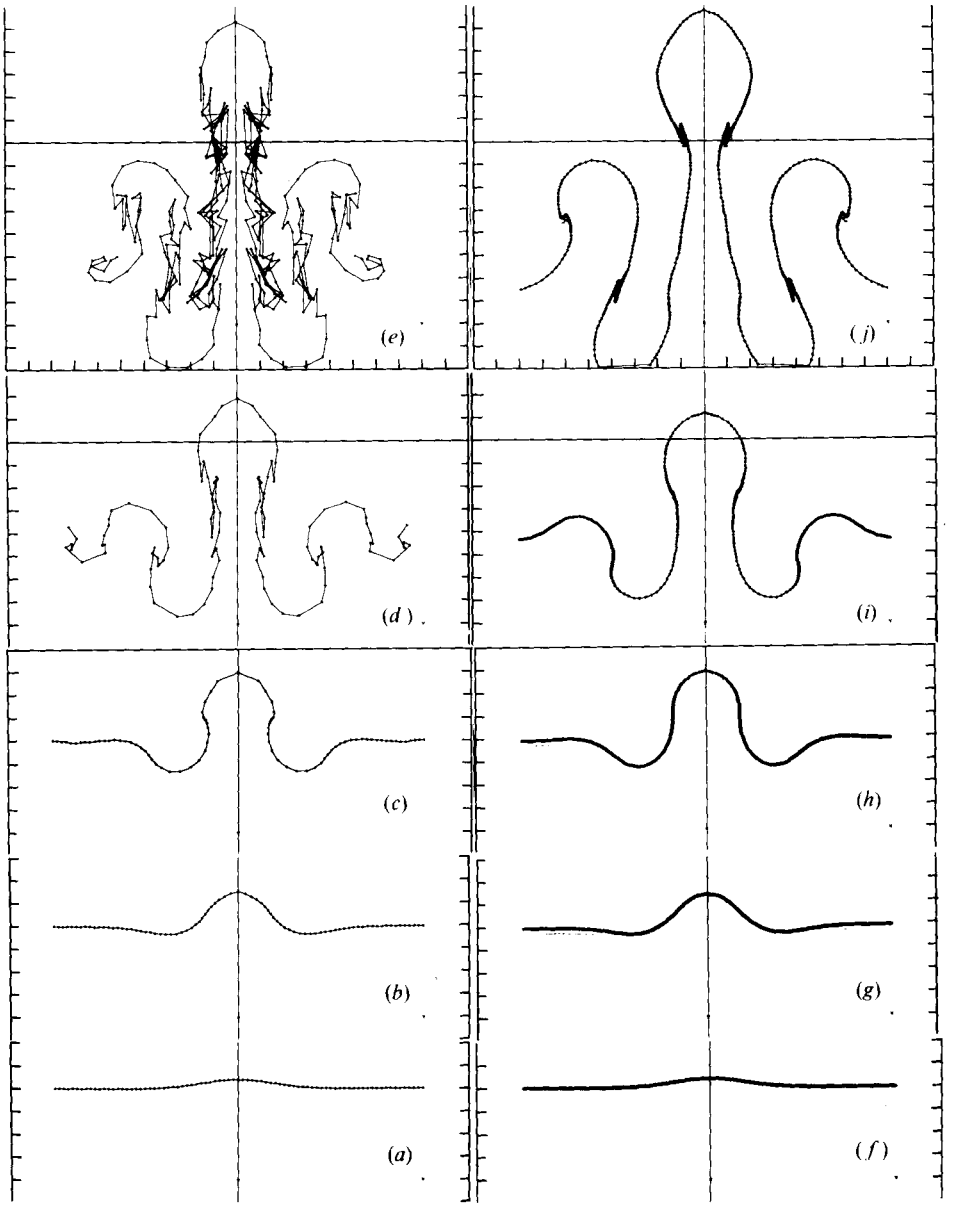

FIGURE 4. Saffman–Taylor instability. (*a*)–(*e*) Results of Green's function method. (*f*)–(*j*) Results of VIC method. Non-dimensionalized time (defined in §2.3): (*a*), (*f*) 0; (*b*), (*g*) 0·22; (*c*), (*h*) 0·38; (*d*) 0·68; (*i*) 0·60; (*e*), (*j*) 0·98.

already mentioned in the introduction, are an oil/water interface in sand or in shale, and a fresh-air/smoke interface in a peat moss or a granular coal bed fire. As is illustrated by the general equation (10), such a situation involves two diffusive gradients, and the corresponding flow system is called a doubly diffusive system.

To illustrate how the Saffman–Taylor instability evolves in reality, results of two numerical simulations, using the Green's function and the VIC method, are shown in

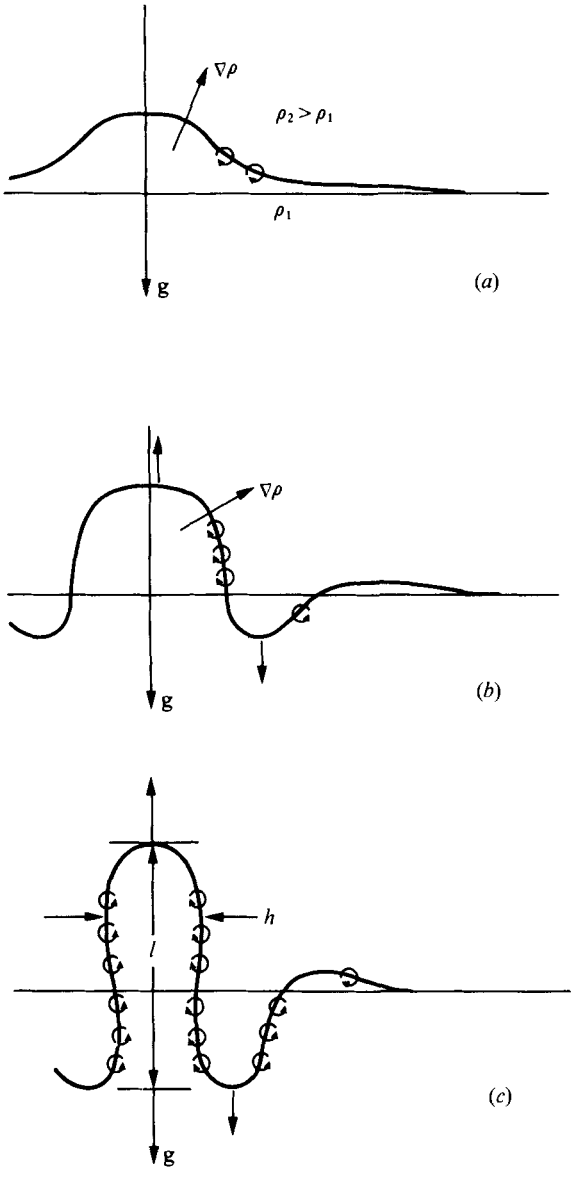

FIGURE 5

figures 4(*a*)–(*e*) and 4(*f*)–(*j*) respectively. An interface in a porous medium separating two fluids of different density, kinematic viscosity or both is perturbed by a Gaussian displacement profile at the centre (figures 4*a*,*f*). Forty-one and 281 vortices, respectively, were used on the right half-plane to represent the interface. Figures 4(*b*) and (*g*) show that the centre has risen while the outer edges are depressed. Figures 4(*c*) and (*d*), and (*h*) and (*i*) show the continual rise of the centre and fall of the outer edges. Figure 4(*c*) also shows that as the finger grows the spacing between vortices on the top becomes large, so that unless a method by which vortices can be added to this region is implemented one cannot obtain good resolution there. Notice that, in

figure 4 (*d*) at $\tau = 0{\cdot}68$, one vortex has been added to the centre region as a result of the repacking procedure explained in §3.1. Development of smaller-scale 'fingers' can be seen in both figure 4 (*e*) and figure 4 (*j*), near and behind the advancing main 'fingers'. Its physical origin, however, has not been investigated. Saffman & Taylor (1958) studied the fingerlike structure in a Hele Shaw cell and found that the ratio of the width of the fingers to their spacing is almost always equal to $\frac{1}{2}$, which is also demonstrated by figures 4 (*e*) and (*j*). The total number of vortices at $\tau = 0{\cdot}98$ in figures 4 (*e*) and (*j*) are 146 and 218 respectively. In summary, both methods yield similar large-scale results at $\tau = 0{\cdot}98$, although at this time an image effect is seen in figure 4 (*j*). The difference in the small-scale result is attributed to the difference between the core radius $r_c = 0{\cdot}05$ for the Green's function and the zero core radius and finite mesh size $\Delta x, \Delta y = 0{\cdot}125$ and $M_x = M_y = 32$ for the VIC method. Further continuation of numerical calculation by either method is not warranted since it becomes costly for the Green's function method ($N = 146$ at $\tau = 0{\cdot}98$) and a more significant image effect will be apparent for the VIC method.

Although numerical simulation of this problem on a quantitative basis has not been obtained, a qualitative understanding of the physical phenomenon can be derived from the numerical result. For simplicity, let us assume $\Delta\mu \equiv 0$, so that the flow is characterized by two quantities: the acceleration $g\Delta\rho/\rho$ and the viscous stress operative in a porous medium with porosity $\kappa = \frac{1}{8}d^2$. A balance between the gravitational force and the viscous force will lead to an equilibrium state where a terminal velocity u_t exists. We shall estimate u_t and the final interface configuration at the equilibrium stage.

First, suppose that the finger is replaced by a sphere of fluid accelerated under the effective gravitational force $g\Delta\rho/\rho$ and decelerated by the viscous force $\nu\nabla^2 u \sim \nu u_t/\kappa$ times the surface area of the sphere. Then one finds $u_t \cong \frac{4}{3}g\,(\Delta\rho/\rho)(\kappa/\nu)$.

Second, from figure 5, one finds that the vorticity generated is that due to the terms $(\kappa/\nu)\,(\nabla\rho/\rho_0) \times \mathbf{g}$ only, i.e. the vorticity is a maximum where $\partial\rho/\partial x$ is a maximum. The resultant motion will be to lift up the centre and push down the edges. At some later time, as is shown in figure 5 (*b*), vorticity of the opposite sign also appears, but the resultant motion is a further acceleration in the same direction as in the initial stage. Assuming that the final stage of the finger structure is that depicted in figures 4 (*e*) and 5 (*c*), we can estimate the velocity at the centre fingertip owing to the vortices distributed on the long vertical interface. Let l be its length and h its width; we find

$$u_t \sim \frac{2}{\pi}\int_0^{\frac{1}{2}l} \frac{d\Gamma}{(x^2+y^2)^{\frac{1}{2}}} \sim \frac{2\kappa}{\nu\pi}\frac{g\Delta\rho}{\rho}\ln\left(\frac{l}{h}\right).$$

Identifying this relation with that obtained by the first method, one finds $l \cong 8h$, which is in agreement with the numerical results shown in figures 4 (*e*) and (*j*).

4.3. *Transport of aircraft trailing vortices in a wind shear*

The limitation on any numerical scheme for studying this problem is its small time step. This time is determined by the peak angular velocity around the trailing vortices. Since angular velocities exceeding 10 rad/s are expected in practical cases, the time step required to follow this motion would be substantially less than 0·1 s. To cover an elapsed time of 100 s requires more than 1000 steps. This is excessive, and it is desirable

to obtain a numerical scheme that can handle a large number of discrete vortices without the limitations of a small integration time step.

There is another reason why a pure VIC method will not be adequate. In order to resolve a trailing-vortex flow field that has a core radius of a few metres, one must have a mesh smaller than the core radius. On the other hand, one must cover an overall distance determined by the product of the wind speed and the total elapsed time of interest (several hundred metres). The ratio of this dimension to the core radius indicates that at least 100 mesh points in each direction are required to resolve the flow field; this is large even for the CDC 7600 computer. To achieve an economical and accurate computation, we introduce a hybrid method that is capable of resolving the fine structure near the trailing vortices while maintaining a relatively coarse mesh.

We use the fact that the vortex sheet quickly turns into two (or more) well-defined localized structures which maintain their identity (trailing vortices) for many rotations. The total velocity field is taken to be a superposition of two parts: one the contribution of the localized trailing vortices and the other due to the distributed vorticity (wind-shear vortices). The velocity field of the trailing vortex is constructed from an axisymmetric model. This model in general requires values of two quantities to be specified: the total vortex circulation $\Gamma(t)$ and a characteristic radius r_c (typically the core radius). Both Γ and r_c are functions of time. In the present simulation we use the model constructed by Owen (1970) for a turbulent vortex, in which $r_c = (2/\sigma)(\nu t)^{\frac{1}{2}}$ and $\sigma = \Lambda^{-1}(\nu/\Gamma_0)^{\frac{1}{2}}$, where ν is the kinematic viscosity, Γ_0 is the total circulation over one wing and Λ is a numerical constant of order unity (set equal to unity in the present simulation). A simple laminar diffusion profile is used for the radial distribution of circulation: $\Gamma[1-\exp(-r^2/r_c^2)]$. As the core expands, the distributed vortices are captured and incorporated into the tip vortices. The trailing-vortex locations are updated to the centroid of the original vorticity distribution in this capture process. The velocities due to the trailing vortices and the wind shear are then superposed.

In this paper we avoid the 'short time step' problem by superposing displacements rather than velocities. The angular displacements directly induced by the trailing vortices are evaluated. This displacement is then added to that due to the slowly varying background velocity field. By repeating this process at each time step, one follows accurately the motion near the core even though a given point may rotate several times about the trailing vortex during one time step. This method is called the hybrid VIC method.

By wing theory, the lift or wing loading is linearly proportional to the circulation about the wing cross-section, and it is well known that for simple wings of high aspect ratio the wing loading can be approximated by the elliptic curve

$$S(x)/S_0 = [1-(x/R)^2]^{\frac{1}{2}},$$

where S_0 is the maximum circulation at $x = 0$ and R is the wing span. The circulation between the points x and $x+dx$ is decreased by the amount $\Delta S = S(x+dx)-S(x)$ and this amount of circulation must be shed from the wing section between these two points. Thus the circulation of the trailing vortex sheet at any point x is equal to the rate of change of $S(x)$, i.e. $-dS(x)/dx$, along the wing.

To model this initial velocity field we divide the vortex sheet into a number of strips in the flight direction, each having a circulation $\Gamma_i(x)$ given by

$$\Gamma(x_i) = [S(x_i)-S(x_{i+1})]/\Delta x, \tag{15}$$

where $\Delta x = x_{i+1}-x_i$.

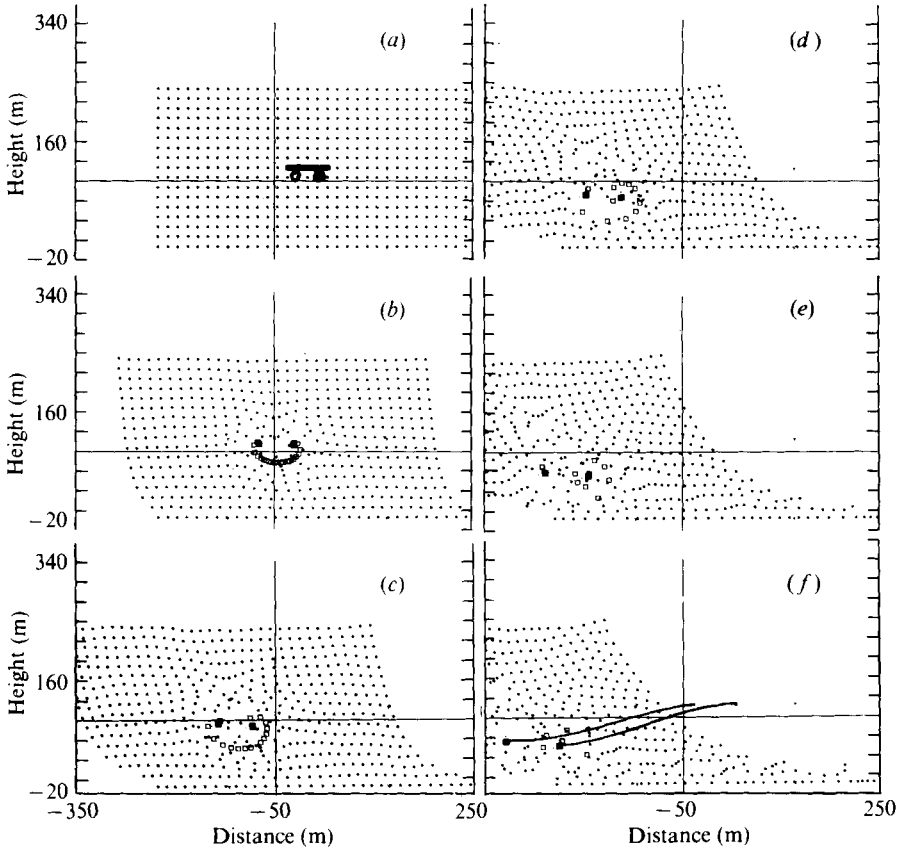

FIGURE 6. Transport of aircraft trailing vortices in a crosswind shear. Time: (*a*) 0; (*b*) 7 s; (*c*) 17 s; (*d*) 27 s; (*e*) 37 s; (*f*) 47 s. ●, Wind-shear vortices; □, vortices on trailing vortex sheet; ■, 'tip vortices'.

The real lift distribution deviates considerably from the elliptic loading rule, as was pointed out by Donaldson, Snedeker & Sullivan (1973). Although the real profiles can be treated easily by the present model, we have applied the elliptic loading rule for its-simplicity.

The wind profile near the ground in a neutrally stable atmosphere is known to exhibit a logarithmic dependence upon the height y (Blackdar & Tennekes 1968):

$$U = \frac{u_\tau}{\kappa} \ln\left(1 + \frac{y}{y_0}\right) + \text{constant},$$

where u_τ is the friction velocity and is usually related to the wind velocity by $u_\tau \cong \frac{1}{30}U$ (at a standard height). The parameter κ is the Kármán constant (Hinze 1959, p. 619) and is equal to 0·42. The parameter y_0 is the roughness height.

From the preceding equation the vertical wind shear can be obtained by taking the derivative with respect to y:

$$\zeta(y) = u_\tau/\kappa y.$$

To describe the mean wind-shear field, this circulation is assigned to a uniform distribution of discrete vortices as follows:

$$\Gamma_0 = \frac{U_\tau}{\kappa} \ln\left(1 + \frac{\Delta y}{2y_0}\right) \Delta x$$

for the ground layer and

$$\Gamma_j = \frac{U_\tau}{\kappa} \ln\left(\frac{Y_j + \frac{1}{2}\Delta y}{Y_j - \frac{1}{2}\Delta y}\right) \Delta x, \quad j = 2, \ldots, N, \tag{16}$$

for layers above ground, where Δx and Δy are the horizontal and vertical mesh sizes and N is the total number of rows of vortices; $N = 17$ for this study. The present treatment is similar to that of Brashears & Hallock (1973) except for the number of wind-shear vortices used to simulate the wind-shear field and the VIC method. In the present analysis, the use of the mixed Eulerian–Lagrangian (hybrid vortex-in-cell) method allows a highly detailed spatial resolution of the wind field at relatively modest cost.

The trailing vortex shed from a Boeing 747 aircraft at a height of 120 m above the runway was studied with a 32×32 grid. The trailing vortex was represented by 25 discrete vortices over half of the wing span, each being assigned a circulation according to (15). The wind-shear vorticity [or circulation by (16)] is assigned on 544 vortices (dots in figure 6) over the flow domain on a 17×32 mesh, and the images are obtained by the symmetry condition in the vertical direction. The buoyant engine exhaust can also be represented by 25 vortices, with a small temperature difference from the ambient air. However such an option was not used in this calculation. Figure 6(*a*) shows the initial geometry of a Boeing 747 trailing vortex sheet (open squares) and its buoyant exhaust. Figure 6(*b*) shows the rolling up of the vortex sheet after 7 s, as some of the discrete vortices are captured by the trailing vortices (two solid squares). Figure 6(*c*) shows the overall picture of the vortex system at $t = 17$ s: the wind-shear vortices near the ground, where the vorticity is maximum, are swept up and mutual induction between these wind-shear vortices and the localized tip vortices may be expected to emerge. Figure 6(*d*) shows the skewed configuration due to the wind shear at $t = 27$ s. The trailing vortices have been transported nearly 170 m to the left from their original position, and the positions of the wind-shear vortices delineate the wind-shear profile. Figure 6(*e*) shows the location of the vortices at $t = 37$ s; the downwind (left) vortex is observed to rise as a result of the interaction with the wind shear. The trajectories of the two trailing vortices are marked in figure 6(*f*). A more detailed discussion of the problem is given by Thomson & Meng (1976).

4.4. *Gravity current*

We now turn to a phenomenon which is commonly treated as a hydraulic-jump problem rather than from the point of view of the vortex interactions. It corresponds to the intrusion of a heavier fluid (a front or 'nose') into a fluid of smaller density. Examples of this flow are found in the atmosphere: in a weather front (say, a sea breeze) and in front of a gravity current, which is usually termed a 'Sudanese haboob'. Examples in the ocean are the flow near a river–sea junction and the intrusion of salt water under fresh water when a lock gate is opened. Many experiments have been made to study this phenomenon. A summary can be found in Turner (1973, p. 71). Benjamin (1968) showed that the head of the front must be followed by a turbulent region and an abrupt drop to a layer of uniform depth. Kármán (1940) showed that the inclination of the nose (or head) at the front is 60° to the horizontal.

In this study we shall resolve the nonlinearity of the problem from an idealized vorticity interaction point of view. An idealized weather front, or a mixed region of

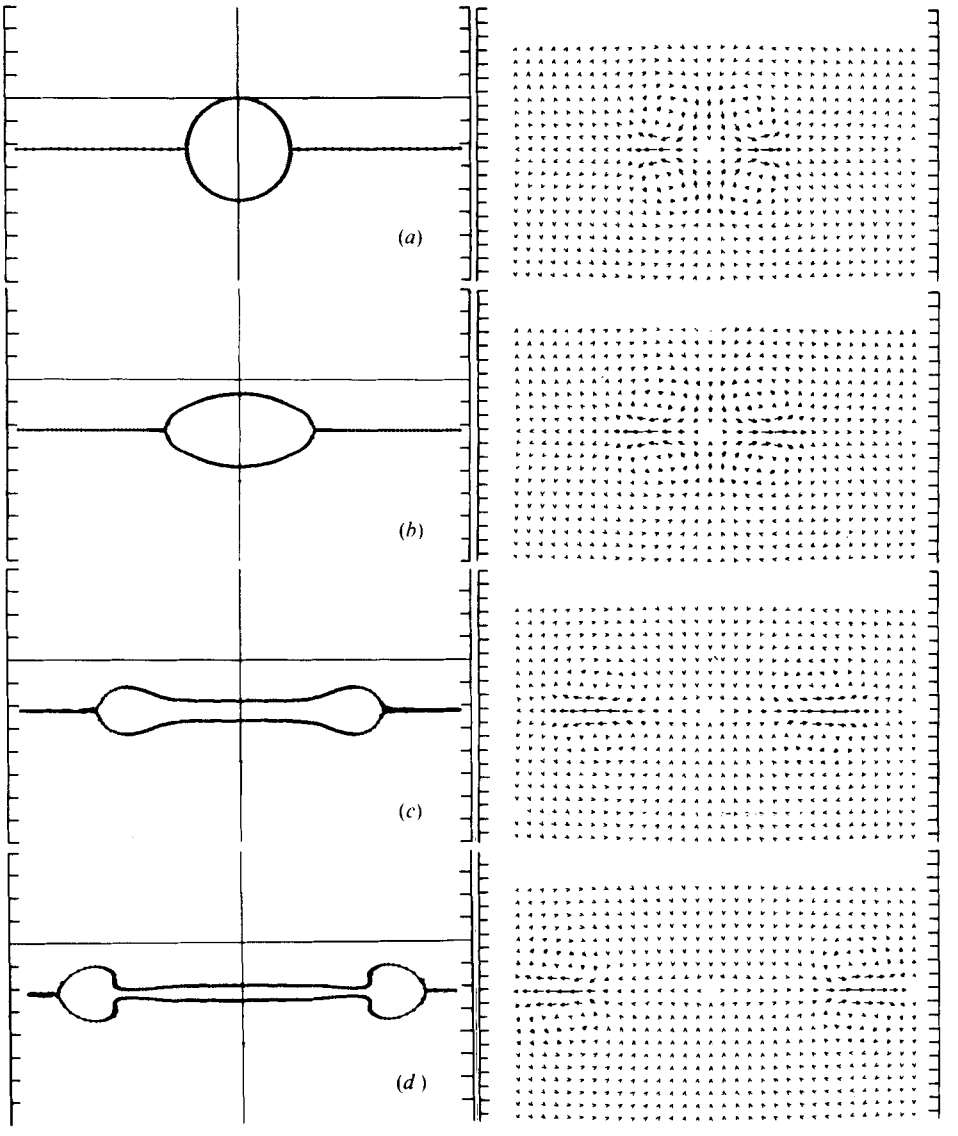

FIGURE 7. Formation of a gravity current. Results obtained by VIC method with 171 vortices on the first quadrant. The left column shows evolution of the interface, the right the corresponding velocity distribution. Non-dimensionalized time (defined in §2.3): (*a*) 0; (*b*) 0·60; (*c*) 1·60; (*d*) 2·20. Maximum non-dimensionalized flow speed: (*a*) 0·120; (*b*) 1·638; (*c*) 2·169; (*d*) 2·136.

constant density (Wu 1969), is represented by a circular cylinder of constant-density (ρ_0) fluid lying on a stable density discontinuity, with densities $\rho_0 \pm \Delta\rho$ above and below the interface. Vorticity generated along the interface and its self-interaction will dominate the subsequent rotational motion. The VIC method, with 171 discrete vortices along the interface, will be applied since the Green's function method is not practical for such a large number of vortex elements. The evolution of the advancing head and its advancing speed will be analysed and compared with the theoretical analyses.

Figure 7(*a*) shows the initial geometry and its velocity-vector plot. A circular cylinder of fluid of intermediate density is located on a stably stratified density discontinuity. The dots show the location of the vortices: 171 points altogether, distributed non-uniformly over the first quadrant, with the higher number density near the interface (or the thermocline) and the smaller on the cylinder top. This was necessary to ensure a good resolution of the nose geometry. The vorticity was initially zero everywhere. Then (11)–(13) were applied to advance the calculation. Owing to the lower fluid density above the cylinder and the higher underneath, the buoyant force will flatten the cylinder; if there were no vorticity generated, the circular cylinder would simply be flattened into a thin layer. Owing to the vorticity generated by the density difference across the cylinder and the symmetry condition in the vertical direction, it forms a self-advancing vortex pair (see the vector plot in figure 7*a*). The nose is commonly known as the gravity current or weather front in meteorology. Notice that the maximum velocity at $\tau = 0$ is

$$0{\cdot}12\left(g\frac{\Delta\rho}{\rho_0}\frac{R}{2\pi}\right)^{\frac{1}{2}}.$$

Figure 7(*b*) shows (for $\tau = 0{\cdot}6$) the flattening cylinder and its velocity distribution. The velocity has grown to

$$1{\cdot}6\left(g\frac{\Delta\rho}{\rho_0}\frac{R}{2\pi}\right)^{\frac{1}{2}}.$$

Figure 7(*c*) shows the nose shape at $\tau = 1{\cdot}6$. The nose has a slope with a half included angle of nearly 60° as was predicted by Kármán (1940). He also predicted that the nose's advancing velocity is bounded by $1/2^{\frac{1}{2}} \leqslant v/[g(\Delta\rho/\rho)H]^{\frac{1}{2}} \leqslant 2^{\frac{1}{2}}$ if the ratio of the depth H of the intruding layer to the depth d of the overlying layer is bounded by $\frac{1}{2} \geqslant H/d \geqslant 0$. Since $H \cong R$ for the present calculation, one can estimate from the above relation that the maximum velocity (the velocity at the nose) should be bounded by

$$\left(g\frac{\Delta\rho}{\rho_0}\frac{R}{2}\right)^{\frac{1}{2}} \quad \text{and} \quad \left(g\frac{\Delta\rho}{\rho_0}2R\right)^{\frac{1}{2}},$$

which agrees with what is shown in the velocity-vector plots at $\tau = 1{\cdot}6$ and $2{\cdot}2$. The solution at $\tau = 2{\cdot}2$ is given in figure 7(*d*), which shows a well-developed nose advancing at a constant speed

$$\approx 2{\cdot}1\left(g\frac{\Delta\rho}{\rho_0}\frac{R}{2\pi}\right)^{\frac{1}{2}}.$$

5. Conclusion

We have shown that a special class of nonlinear hydrodynamic flows including a density interface can be studied by discrete vortex element methods. These numerical methods exploit the basic rotationality (which introduces the nonlinearity) of the physical problem and make possible a simple explanation of the observed phenomena. Application of this method to study many other practical problems is quite possible. Extensions of the basic approach to three space dimensions and a large density difference across the interface will be explored in the future.

REFERENCES

BENJAMIN, T. B. 1968 Gravity currents and related phenomena. *J. Fluid Mech.* **31**, 209.

BLACKDAR, A. K. & TENNEKES, H. 1968 Asymptotic similarity in neutral barotropic planetary boundary layers. *J. Atmos. Sci.* **25**, 1015.

BRASHEARS, M. R. & HALLOCK, J. N. 1973 Aircraft wake vortex transport model. *A.I.A.A. Paper* no. 73–679.

CHORIN, A. J. & BERNARD, P. S. 1973 Discretization of a vortex street with an example of roll-up. *J. Comp. Phys.* **13**, 423.

COOLEY, J. W. & TUKEY, J. W. 1965 An algorithm for the machine calculation of complex Fourier series. *Math. Comp.* **19**, 297.

DONALDSON, C. DUP., SNEDEKER, R. S. & SULLIVAN, R. D. 1973 Calculation of the wakes of three transport aircraft in holding, takeoff, and landing configurations, and comparison with experimental measurements. *Air Force Office Sci. Res. Wash. Rep.* AFOSR-TR-73-1594 (also FAA-RD-73-42).

FINK, P. T. & SOH, W. K. 1974 Calculation of vortex sheets in unsteady flow and applications in ship hydrodynamics. *Univ. New South Wales Rep.* NAV/ARCH 74/1.

FOHL, T. 1967 Optimization of flow for forcing stack wastes to high altitudes. *J. Air Pollution Control Ass.* **17**, 730.

HINZE, J. O. 1959 *Turbulence.* McGraw-Hill.

KÁRMÁN, T. VON 1940 The engineer grapples with nonlinear problems. *Am. Math. Soc. Bull.* **46**, 615.

MENG, J. C. S. 1977 The physics of vortex ring evolution in a stratified and shearing environment. *A.I.A.A. Paper* no. 77-12.

OWEN, P. R. 1970 The decay of a turbulent trailing vortex. *Aero. Quart.* **21**, 69.

SAFFMAN, P. G. & TAYLOR, G. I. 1958 The penetration of a fluid into a porous medium or Hele-Shaw cell containing a more viscous liquid. *Proc. Roy. Soc.* A **245**, 312.

SCORER, R. S. 1958 *Natural Aerodynamics.* Pergamon.

THOMSON, J. A. & MENG, J. C. S. 1976 Scanning laser doppler velocimeter system simulation for sensing aircraft wake vortices. *J. Aircraft* **13**, 605.

TURNER, J. S. 1959 A comparison between buoyant vortex rings and vortex pairs. *J. Fluid Mech.* **7**, 419.

TURNER, J. S. 1973 *Buoyancy Effects in Fluids.* Cambridge University Press.

WOODS, J. D. 1969 On Richardson's numbers as criteria for laminar–turbulent–laminar transition in the ocean and atmosphere. *Radio Sci.* **4**, 1289.

WU, J. 1969 Mixed region collapse with internal wave generation in a density-stratified medium. *J. Fluid Mech.* **35**, 531.